Cold Test #2
Spartan IR Camera for the SOAR Telescope

Dustin I. Baker
Edwin D. Loh

Department of Physics & Astronomy
Michigan State University, East Lansing, MI 48824

Loh@msu.edu 517 355–9200 x2480

19 October 2006

Abstract

For the second cold test of the instrument, we installed the 4-detector assembly and an infrared detector in the instrument for the first time. We measured the dark current, photon noise, the noise power spectrum, flexure of the wide-field channel, and image quality. We tested the 4-eyed mechanism for wear. We discovered these problems. (1) Three limit switches failed. (Limit switches are the positional references for the mechanisms.) (2) The dark current is so high that it is larger than the sky background in the J band. We believe that this is caused by openings in the multi-layer insulation for the detector cables that admits radiation (at $\lambda 2.5\mu$) from the warm vacuum enclosure. (3) The Strehl ratio (defined here as the amount of light in the central pixel relative to that computed for a diffarction image) is 0.6–0.7 for both the wide-field and high-res channels at $\lambda 1.523\mu$m. We do not understand why the Strehl ratio in the infrared is lower than our measurement at $\lambda 0.632\mu$m, since the effect of positional or fabrication errors δ scale as δ/λ. (4) Some of the quartz strings that drive the 4-eye mechanism are worn: a few strands are broken. We discovered that some of the rounded holes for the strings have sharp transitions. (5) A noise at 120 Hz and multiples of it are visible. (6) An unaccounted 2-pixel movement of the image occurred over the first 6.5 hr of the flexure test; over the next day, the flexure was sinusoidal with orientation of the instrument.

Contents

1 Dark current

We measured the dark current (Figure 1) by inserting the dark slide, which is at pupil stop. The instrument is cold, and the surrounding are at 290 K. The detector temperature is 83 K.

The dark current is a very high. It is a factor of 1000 higher than Rockwell's design goal at 77 K. The difference in temperature accounts only for a factor of 12.

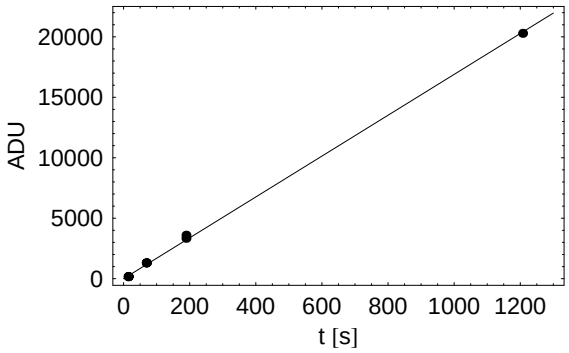

Figure 1: Dark current of detector #14 at 83 K. The slope is 17 ADU/s (65 e^-/s).

The high dark current degrades the performance of the instrument. (1) The dark current is a factor of 4 higher than the expected sky background in the J-band filter for the high-resolution channel (the darkest broad-band case). Therefore the limiting magnitude is 0.9 mag worse for

background-limited observations for that case. (2) The noise from the dark current exceeds the detector noise for exposures longer than 2 s. For narrow-band observations where the detector noise should dominate, there is degradation for practical exposure times.

1.1 Light leak

Light leaks between the warm outside and the detector may account for the dark current. The detector sees radiation for which the wavelength $\lambda < 2.5\,\mu$m.

There are two openings in the multi-layer insulation for the detector cables (Figure 2). The openings are cross shaped slits. The slits were not taped shut for this cold test. We estimate the openings are $25 \times 12\,\mathrm{mm}^2$.

First we model the light to fill a spherical volume with a radius of 260 mm, which has the same volume as the chamber that the detector sees directly. The light from the openings first strikes a brightly anodized, matte finished cover, which has a high reflectivity. We use a reflectivity of 12% for black anodized aluminum at a wavelength 2500 nm[1] After two reflections off of black-anodized surfaces, the light can reach the detector. The measured light leak is a factor of 20 greater than the model.

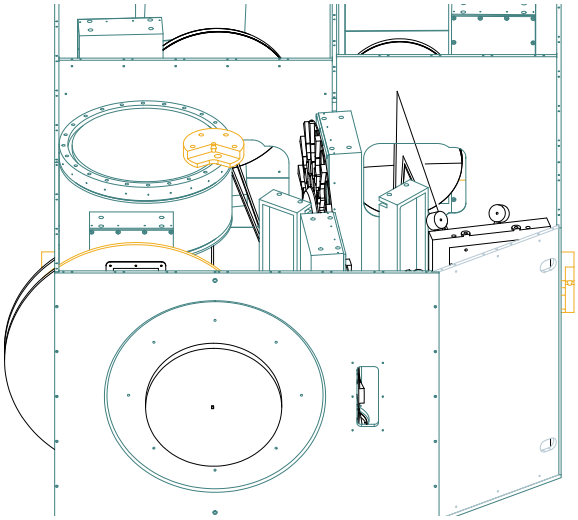

Figure 2: The cryo-optical box and the optical components. Two openings on the right are for cables to the detector. The openings for cables in the multilayer thermal insulation admit 294-K radiation, the short wavelength part of which is visible to the detector.

Second, there is a path between the opening and surfaces that the detector sees. Although this path is open for a small fraction of the light, only one reflection is needed. The measured light leak is brighter by a factor 2. Because of the rough nature of the model, we conclude this is the likely dominant path of the light leak.

A second opening is the entrance of the instrument. Since stray light must pass through the Lyot stop, the light must make

[1]GNIRS SDN 0003.24–Surface Treatments (no author, undated) quotes *Handbook of Optics*.

several reflections off of black surfaces to get to the detector. We discovered four leaks between two chambers upstream and downstream of the Lyot stop. We measured the effect of this leak. We used a 400-1000 nm sensor placed at the location of the detector. A light bulb was placed off of the field and about 200 mm from the entrance of the instrument. This leak is a factor of 10 less than the leak of the cable opening. After blocking the leaks, we could detect no light, and the upper limit is a factor of 100 lower than the amount with the unblocked leak.

Openings in the cryo-optical box to the space between it and the multilayer insulation are not viable as the source for the light leak. Since the temperature of that region is 160 K, the thermal radiation is a factor of 10^7 less than that at room temperature.

2 Rotation Stages

2.1 Binding

All of the rotation stages do rotate at 77 K; none of them bind up. We are using a Prismatics MDM 2200 motor driver at 1.4 A RMS. (The MDM2200 can supply up to 3 A RMS.) For cold test #1, we used a National Instruments 7604 motor driver, which is limited to 1.0 A RMS. The additional current provides generates 1.4 times the torque, and that is apparently enough to move the rotation stages without binding.

We are still using a NI 7604 motor driver for the mask wheel.

2.2 Limit switches

We are having a problem with the limit switches on three rotation stages. The limit switch allows a rotation stage to be reset to a known location. The little filter wheel, big filter wheel, mask wheel, f/12 camera, and f/21 collimator use rotation stages 000, 02060-097, 02060-098, 02060-099, and 02060-100, respectively.

For rotation stage 099 at 77 K, the reverse limit switch triggered and stayed triggered even when the rotation stage moved away from the reverse limit. The switch released after a few days while we were moving to the forward limit. We took the switch out of the instrument. At room temperature, it is OK. Immersed it in liquid nitrogen, it is triggered even when far from the reverse limit.

For rotation stage 097 at 77 K, the reverse limit switch worked fine for about three weeks, but then it stayed triggered for the last few days of the cold test. We have not tried it at room temperature after the cold test.

The switch on rotation stage 100 triggers at two different positions depending on the starting location. If the starting location is close to the limit switch, the trigger location is farther in the reverse direction, and the limit switch does not untrigger until it is moved far forward. If the starting position is far from the limit switch, the trigger location is close to that at room temperature, and the limit switch untriggers when it is moved forward slightly. This behavior is the same when the rotation stage is immersed in liquid nitrogen. The switch works at room temperature.

We replaced the switches on rotation stages 099 and 100. These rotation stages work now when immersed in liquid nitrogen. We will replace the switch on 098 when Phytron sends replacements.

3 Testing 4-eye

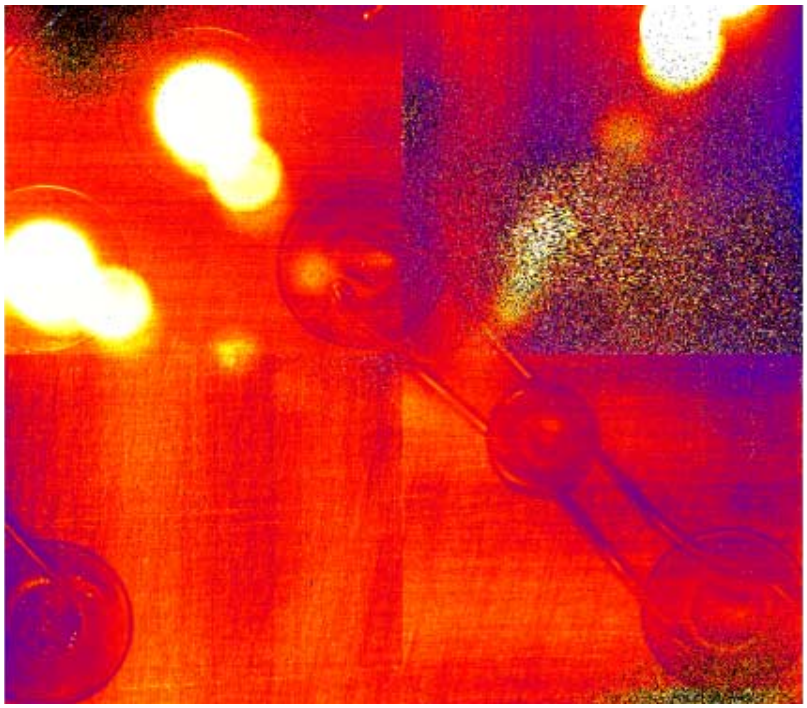

Figure 3: Image of the mask illuminated by thermal radiation from the room. The detector is saturated by the three large openings in the mask; in fact, even the reflections from them are bright. Three pinholes are visible in the upper left, lower left and lower right quadrants. Note the paper clip and screw holding two pinholes.

3.1 First light with 4 eye

We installed engineering-grade detector #14 in position B2 and a multiplexer position A1.

We illuminated pinholes on the mask wheel with ambient radiation(Figure 3).

3.2 Functionality

The question is whether the 4-eye mechanism moves the detector to the mechanical stops, which determine the position of the detectors, at 77 K. The motion is primarily perpendicular to the plane of the detector. We focused in the wide-field mode and then moved 4-eye to the high-resolution mode. The image was still in focus. Therefore the 4-eye mechanism is moving to the stops.

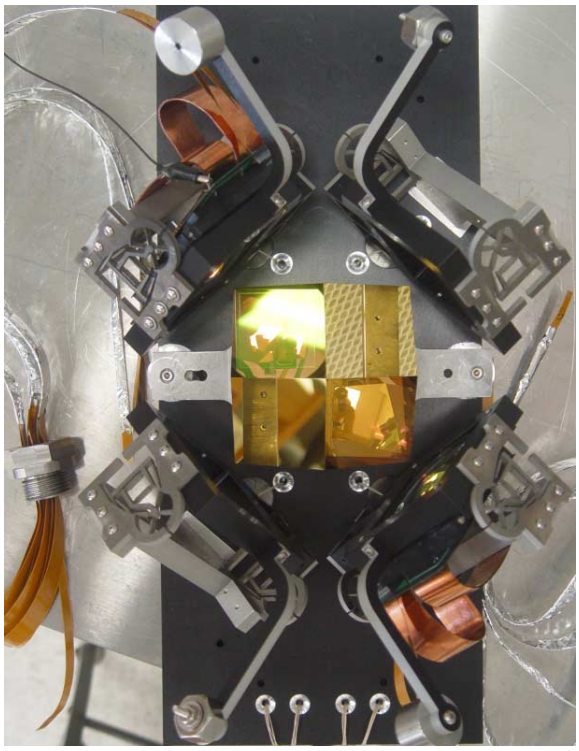

Figure 4: The 4-eye mechanism before installation for cold test #2. Note the Heinen flexible bearings with positioin-defining stops. There are 4 strings exiting the spine at the bottom of the picture.

3.3 Wear test

We moved the 4-eye mechanism from the wide-field position to the high-resolution position and back sixty times while the instrument was cold. When warm, we inspected the quartz strings that connect the f/12 rotation stage and the 4-eye mechanism. A few strands on five strings broke. The fraying occured where the strings run through the 4-eye spine. On the other 7 strings, no strands broke.

The openings in the spine are cut with a corner-rounding end mill, but the transition between the rounded cut and the straight hole is not smooth. (There is an abrupt change in slope.) The transition was removed with a convex, rounded piece of wood covered with #22 metal polish. No fraying occurred with the polished holes at room temperature after running the quartz string back and forth 100 times with 3 times the tension.

4 Flexure

The test is to measure the flexure of the instrument as the direction of gravity changes. Mounted at the Nasmyth position, the Spartan Camera turns about one axis as the telescope tracks a star. For the flexure test, a pinhole on the mask, which is at the focus of the telescope, is illuminated by a laser and imaged on the detector. The flexure test does not reveal flexure of the vacuum enclosure and the A-struts, because the shift between the pinhole and the outside is not measured. The calculated shift due to the A-struts is has an amplitude of 9 m, which is 30 mas in the sky.

A laser illuminates a pinhole, which is placed on the mask plate. We measured the shift of the image of the pinhole (Figure 5) as a function of the orientation of the instrument. The light enters from above at the 0-degree orientation.

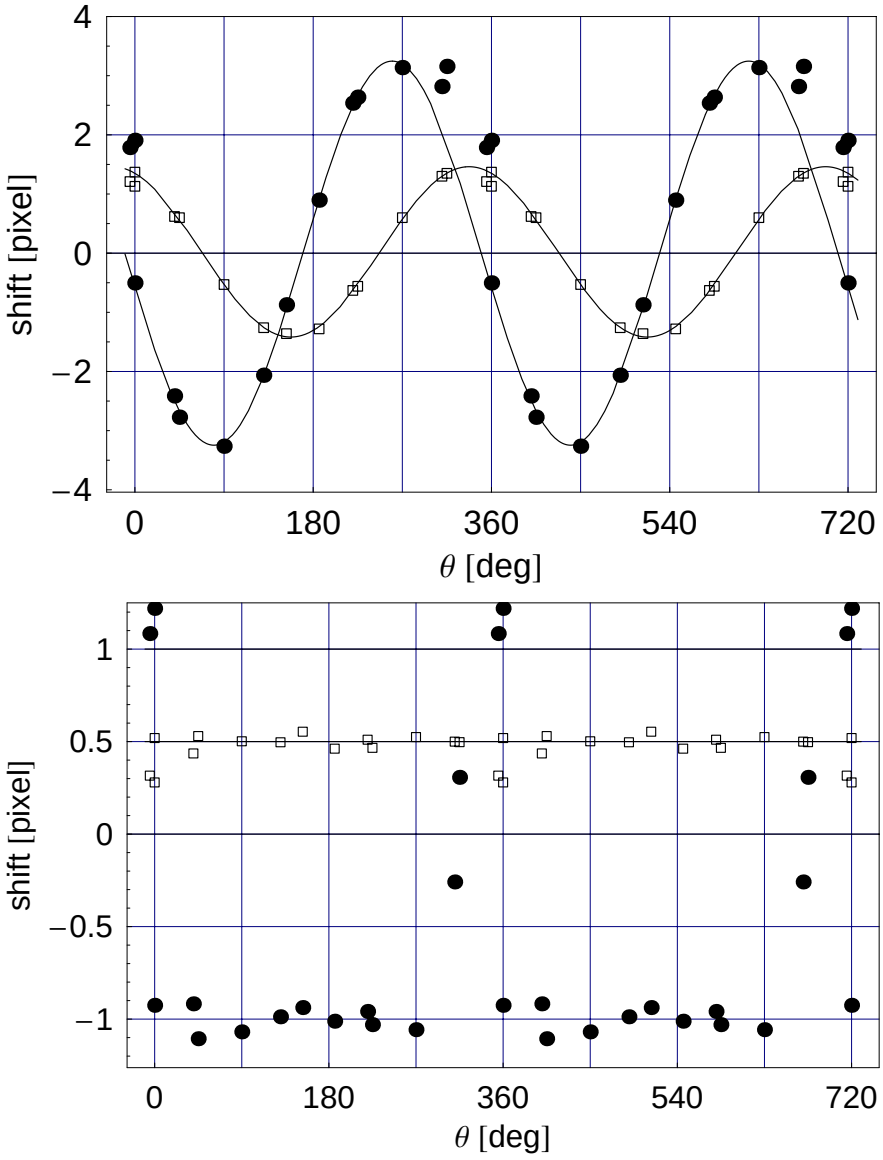

Figure 5: Top–Shift in direction of symmetry (box) and in perpendicular direction (points) vs intrument orientation for the wide field channel at 77K. The first 4 points of the set are ignored in the fit. Bottom–Residual siftted by +0.5 in direction of symmetry (box) and shifted by –1 in perpendicular direction (points) vs intrument orientation for the wide field channel at 77K. the actual residual for the points at the upper edge is 2.5.

5 Power spectrum

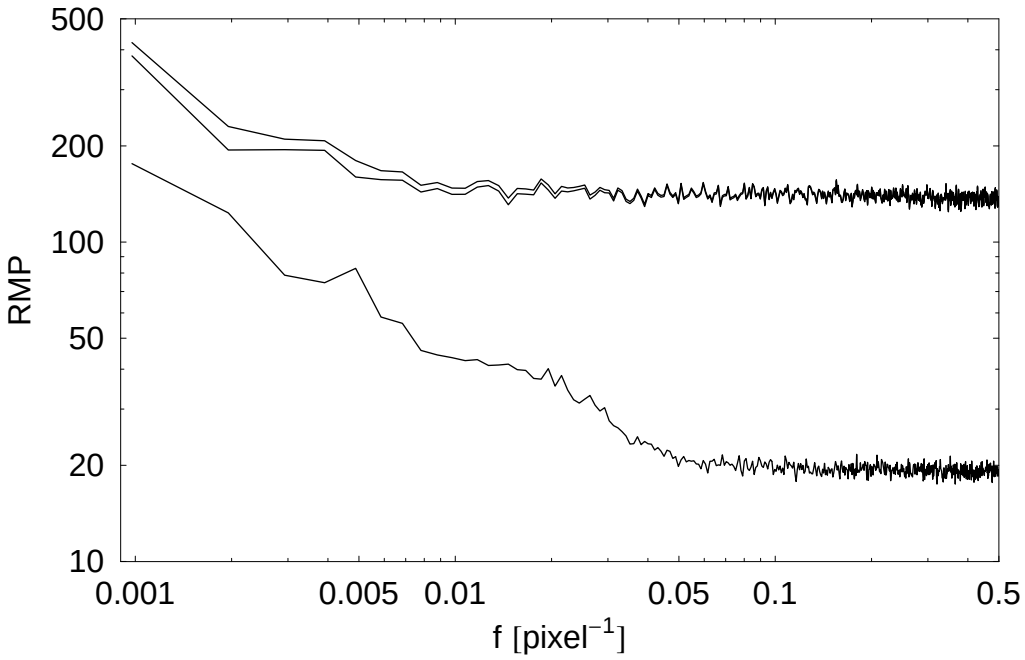

Figure 6: Root-mean-power of rows of a bright image (highest), the bright image with the power of a dark image removed (middle), and a dark image (lowest).

The power spectrum of columns (Figure 7) shows periodic noise. The peaks at 0.0947, 0.1894, 0.2832, 0.3779, 0.4727, and 0.4336 row^{-1} are multiples of 120 Hz aliased by 1, 2, 3, 4, 5, and 5 periods.

The 120-Hz noise may account for some of the low frequency noise in the power spectrum of rows. The fundamental at 0.00085 pixel^{-1} is slightly under the lowest bin at 0.00098 pixel^{-1}; its power is reduced but not completely eliminated. The harmonics all appear unattenuated.

We plan to filter the power before it enters the controller board.

6 Detector memory

The detector has a memory that lasts for 10s of minutes. We have found memory in two types of measurements. (1) After an exposure of a bright star, a dark region appears at the location of the star. The dark region is gone after 30 minutes. (2) In a set of pictures

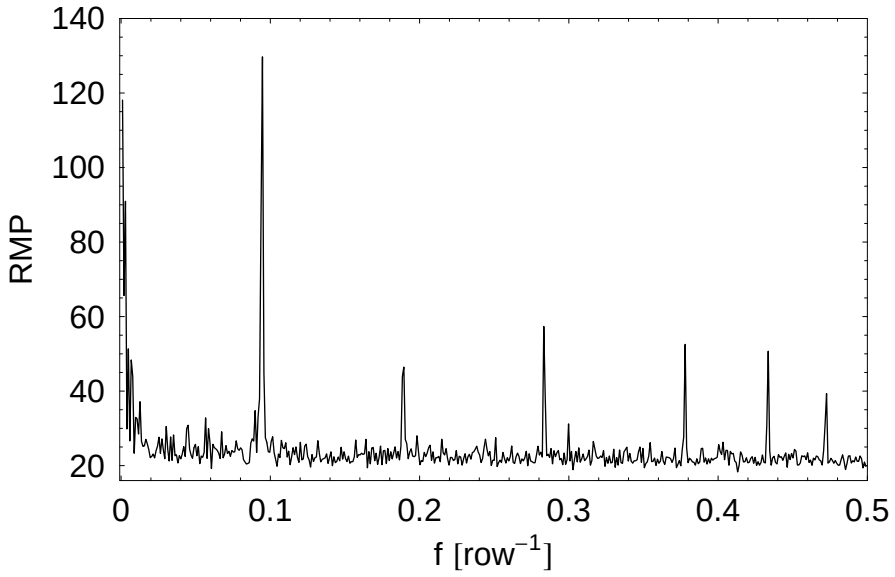

Figure 7: Root-mean-power of columns of a dark image.

with a uniform illumination, the difference between the first two pictures shows higher noise than subsequent pairs.

7 Measurement of amplification and system noise

We took a set of pictures of the room, which is approximately a uniformly illuminated field, to measure the photon noise. Figure 8 is a plot of variance *vs.* median. If the system measured in units of electrons rather than counts of the analog-to-digital converter, the slope would be unity. In order to remove the effects of nonuniformity in illumination, the variance is estimated from the power spectrum of the difference between two pictures where variations smoother than 10 pixels were ignored.

The conversion from electrons to counts is $3.85 \pm 0.02\,\mathrm{e}^-$/count. The noise without light of a long–short pair[2] of pictures is 3.1 ± 0.2 count or $11.8 \pm 0.8\,\mathrm{e}^-$.

[2]The long picture is taken after an exposure; each row in the short one is read immediately after removing the charge. Although the noise in a pixel of each picture is $\frac{1}{2}kT$, the difference is free of that noise.

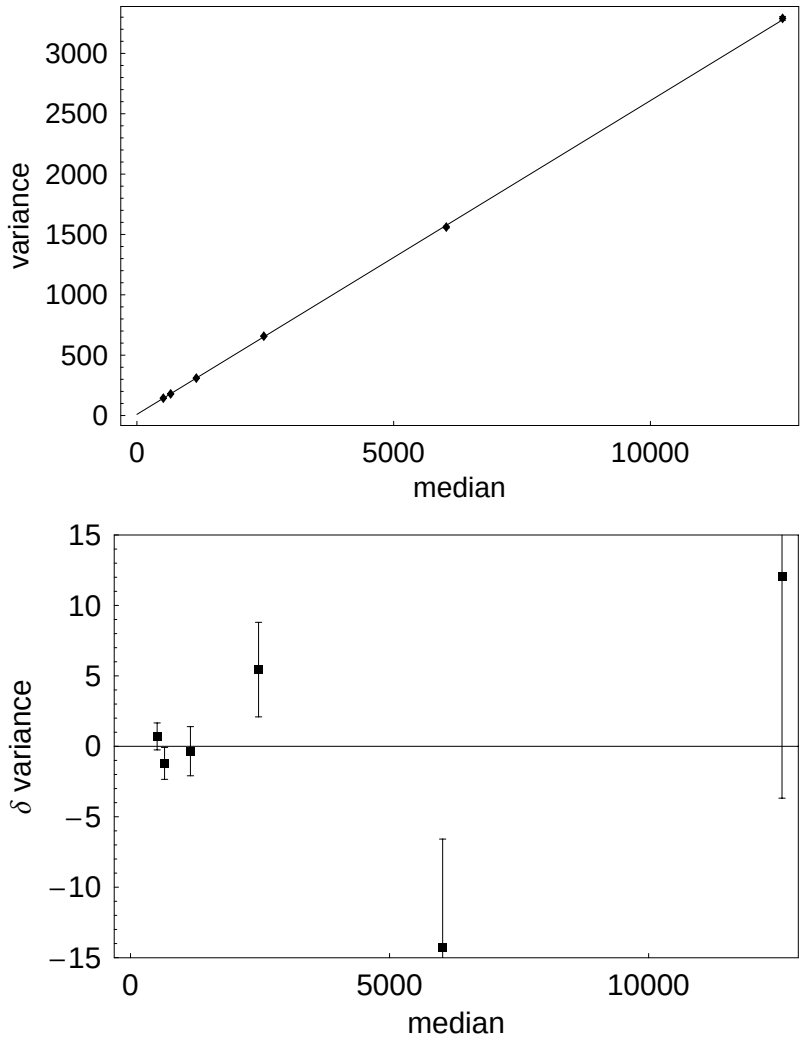

Figure 8: Top panel: Variance *vs*. median for detector #14 at 83 K. The line is the fit with two parameters–noise with no light and photon noise. Bottom panel: Residuals of the fit.

8 Image quality

8.1 Focusing

We use image q, a measure of the image quality in the central 5 pixels, to focus. Image $q_x = (I_+ + I_-)/(I_0 + I_+ + I + -)$ is the fraction of light in the two adjacent pixels in the x-direction compared to that in the central and two adjacent pixels. The definition for q_y is similar.

The data (Figure 9) indicate that the detector needs to move back 0.5 mm from nominal. At the nominal focus, the fuzziness in the x and y directions differ: the image is elongated.

It is possible that we are misinterpreting the image q. The image may be elongated because of a reflection in the 0.38-mm thick sapphire layer on the detector. Changing the focus balances the reflection with abberation. We are changing the focus by rotating the pinhole on the curved mask plate. We are unable to change the focus beyond that shown in Figure 9. For the next cold test, we plan to install a few pinholes with a larger axial offset.

The image q of the high-res channel is very close to that of a perfect image. In the wide-field channel, image q is 0.13 worse than that of a perfect image.

8.2 Strehl

Strictly the Strehl ratio is the light in the center of the image to that for a perfect optic, but here we define it to be the measured light in the central pixel to that computed for a perfect instrument. For the wide-field channel, the central pixel covers more than the center: the half-width of the central pixel, $0.45f\lambda$, where f is the focal ratio. For the high-res channel, the half-width of the central pixel is $0.27f\lambda$.

At 1.53 μ, the Strehl ratio, 0.6–0.7, is considerably lower than our measurement at 0.632 μ, which is 0.83 and 0.75 for the high-res and wide-field channels. We do not understand why.

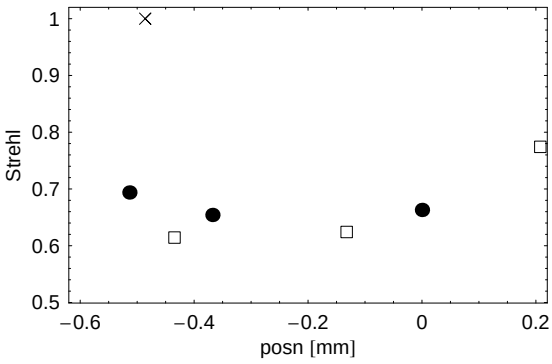

Figure 10: Strehl ratio estimated by the light in the central pixel for the wide-field (points) and high-res (squares) channels vs focus position.

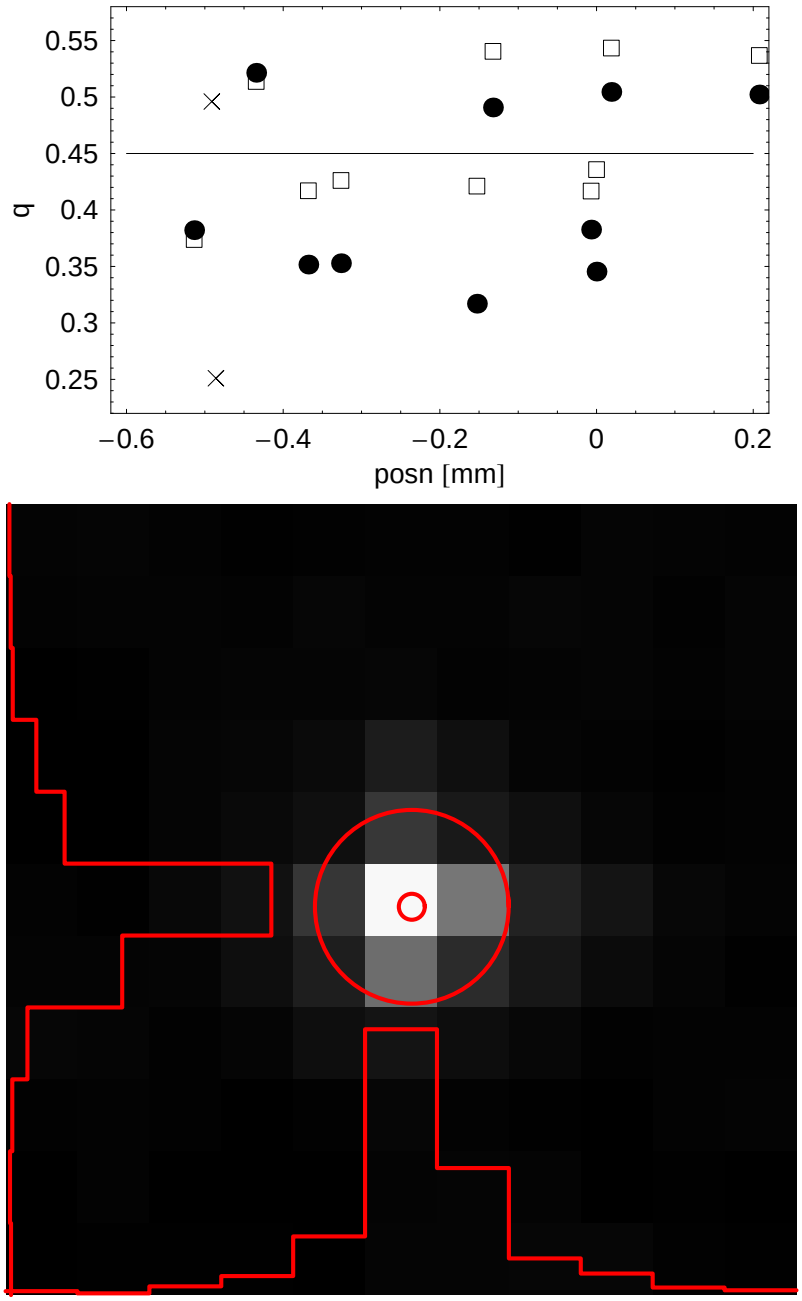

Figure 9: Upper panel–Image q vs axial position of the detector for the high-res (upper panel) and wide-field (lower panel) channels. The points and boxes are for q in perpendicular directions. The crosses indicate q for a perfect diffraction image at the adopted focus. Lower panel–Focused image in the wide-field channel of an 8-μm pinhole illuminated with a 1523-nm laser. The large circle is at the first dark diffraction rings for this picture. The small circle is the geometric image of the pinhole.